PHYSICAL REVIEW B **92**, 220404(R) (2015)

Paramagnetism in the kagome compounds $(Zn,Mg,Cd)Cu_3(OH)_6Cl_2$

Yasir Iqbal,[1,*] Harald O. Jeschke,[2,†] Johannes Reuther,[3,4,‡] Roser Valentí,[2,§] I. I. Mazin,[5,‖] Martin Greiter,[1,¶] and Ronny Thomale[1,#]

[1]*Institute for Theoretical Physics and Astrophysics, Julius-Maximilian's University of Würzburg, Am Hubland, D-97074 Würzburg, Germany*
[2]*Institut für Theoretische Physik, Goethe-Universität Frankfurt, Max-von-Laue-Straße 1, D-60438 Frankfurt am Main, Germany*
[3]*Dahlem Center for Complex Quantum Systems and Fachbereich Physik, Freie Universität Berlin, D-14195 Berlin, Germany*
[4]*Helmholtz-Zentrum Berlin für Materialien und Energie, D-14109 Berlin, Germany*
[5]*Center for Computational Materials Science, Naval Research Laboratory, Code 6390, 4555 Overlook Ave, SW, Washington, DC 20375, USA*

(Received 21 July 2015; revised manuscript received 11 November 2015; published 7 December 2015)

Frustrated magnetism on the kagome lattice has been a fertile ground for rich and fascinating physics, ranging from experimental evidence of a spin liquid to theoretical predictions of exotic superconductivity. Among experimentally realized spin-$\frac{1}{2}$ kagome magnets, herbertsmithite, kapellasite, and haydeeite [$(Zn,Mg)Cu_3(OH)_6Cl_2$] are all well described by a three-parameter Heisenberg model, but they exhibit distinctly different physics. We address the problem using a pseudofermion functional renormalization-group approach and analyze the low-energy physics in the experimentally accessible parameter range. Our analysis places kapellasite and haydeeite near the boundaries between magnetically ordered and disordered phases, implying that slight modifications could dramatically affect their magnetic properties. Inspired by this, we perform *ab initio* density functional theory calculations of $(Zn,Mg,Cd)Cu_3(OH)_6Cl_2$ at various pressures. Our results suggest that by varying pressure and composition one can traverse a paramagnetic regime between different magnetically ordered phases.

DOI: 10.1103/PhysRevB.92.220404 PACS number(s): 75.10.Jm, 75.10.Kt, 75.40.Mg, 05.10.Cc

Introduction. Quantum magnetism in low-dimensional systems with parametric or geometrical frustration has been a highly inspiring field of research ever since the seminal paper of Pomeranchuk [1]. A Holy Grail of the field has been the spin-$\frac{1}{2}$ antiferromagnet on the kagome lattice (Fig. 1), where the geometrical frustration inherent in the individual triangles is only marginally alleviated through a corner sharing lattice pattern [2]. It is widely conjectured to host a spin liquid phase, albeit the nature and the topological classification of this phase are still controversial [3–15]. It may host exotic superconducting phases [16,17].

Recently, significant progress has been achieved regarding experimental realizations of kagome magnets. The couplings in the actual materials, however, differ significantly from idealized models. The most prominent materials are herbertsmithite [$ZnCu_3(OH)_6Cl_2$] [18,19] and its polymorphs, kapellasite [$ZnCu_3(OH)_6Cl_2$] [20,21] and haydeeite [$MgCu_3(OH)_6Cl_2$] [22–26], with ground states ranging from potentially paramagnetic (PM) to weakly ferromagnetic (FM) phases. This variety of ground states in structurally similar systems calls for a thorough theoretical investigation of the experimentally relevant couplings and their implications. In this Rapid Communication, we focus on the following aspects: (1) Which phases—ordered or PM—are realized, depending on Heisenberg couplings J_1, J_2, and J_d (Fig. 1)? (2) What determines the nature of magnetic interactions, and why are they so different in these compounds? (3) Can we deliberately manipulate these materials to probe different parts of the phase diagram, and, in particular, the PM (possibly spin-liquid) phase indicated in Fig. 2?

To begin with, we map out the zero-temperature phase diagram of the J_1-J_2-J_d kagome model. Specifically, we employ the pseudofermion functional renormalization group (PF-FRG) [27–29] method to compute magnetic fluctuations. We find that the experimentally estimated parameters place kapellasite near the borderline between the PM and the antiferromagnetically ordered cuboc-2 phase and haydeeite near the PM/FM border. Using *ab initio* density functional theory (DFT) calculations, we then discuss the reliability of these parameters and possible microscopic origins for their variations. We proceed with suggestions on how one can modify these compounds to shift them away from their current positions and explore other parts of the phase diagram. Among other aspects, our results provide an independent assessment of the initial placement of the materials in the phase diagram.

Herbertsmithite, kapellasite (KL), and haydeeite (HD) feature geometrically perfect Cu^{2+} $S = \frac{1}{2}$ kagome planes with the nearest-neighbor (NN) superexchange J_1 mediated by OH^- and Cl^-. The minimal model also includes subdominant interactions J_2 and J_3 and significant J_d (Fig. 1). Experiment [30] and calculations [31,32] suggest that in herbertsmithite, where only Cu is present in the kagome planes, both J_3 and J_d are negligible, and thus the material is well described by a NN antiferromagnetic model with $J_1 \approx 180$ K, with a small but non-negligible J_2 [29,33]. The quantum paramagnetic ground state of such an antiferromagnet has been intensively studied theoretically (see, e.g., Refs. [3–9, 11–15,34]), and there is experimental evidence of a spin liquid state in herbertsmithite [19,35,36].

On the other hand, in KL and HD, the Zn and Mg ions, respectively, occupy the centers of the Cu hexagons [21], thus spanning the Cu pairs connected by J_d. This seems

*yiqbal@physik.uni-wuerzburg.de
†jeschke@itp.uni-frankfurt.de
‡reuther@zedat.fu-berlin.de
§valenti@itp.uni-frankfurt.de
‖mazin@nrl.navy.mil
¶greiter@physik.uni-wuerzburg.de
#rthomale@physik.uni-wuerzburg.de

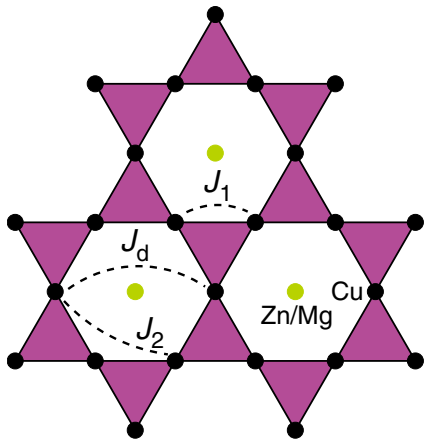

FIG. 1. (Color online) For all kagome magnets considered, the lattice is formed by Cu^{2+} $S = \frac{1}{2}$ spins (black), and the Heisenberg exchange couplings are given by nearest neighbor J_1, second nearest neighbor J_2, and diagonal J_d across the hexagons. Kapellasite and haydeeite feature in-plane Zn^{2+} and Mg^{2+} ions (green), respectively, at the center of the hexagons, triggering appreciable values for J_d.

to explain why the J_d interaction is sizable, and differs considerably between the two compounds. However, the nature of this interaction is probably more complex than that, as discussed in detail in the Supplemental Material [37]. Bernu *et al.* [38] extracted J's in KL from the temperature dependencies of magnetic susceptibility and specific heat, while Boldrin *et al.* [26] did the same for HD, using spin-wave dispersion. With the caveat that these are distinctly different experimental procedures, the estimated exchange coupling constants are $(J_1, J_2, J_d) = (-12, -4, 15.6)$ K for KL [38] and $(J_1, J_d) = (-38, 11)$ K, with $J_2/J_1 \ll 0.1$ for HD [26]. The small and negative values of J_1 signal a large cancellation of the anti- and ferromagnetic contributions to the NN superexchange, which, as we discuss in the Supplemental Material [37], is quite unexpected, but that they are close in both compounds is consistent with their similar geometries. Further investigations using electron spin resonance estimated the symmetric exchange anisotropy D to be only $|D/J_1| \sim 3\%$ [39], thus justifying the use of the (J_1, J_2, J_d) *isotropic* Heisenberg model as a good starting point for both KL and HD.

Model and Methods. The Heisenberg Hamiltonian reads

$$\hat{\mathcal{H}} = J_1 \sum_{\langle ij \rangle} \hat{\mathbf{S}}_i \cdot \hat{\mathbf{S}}_j + J_2 \sum_{\langle\langle ij \rangle\rangle} \hat{\mathbf{S}}_i \cdot \hat{\mathbf{S}}_j + J_d \sum_{\langle\langle\langle ij \rangle\rangle\rangle_d} \hat{\mathbf{S}}_i \cdot \hat{\mathbf{S}}_j, \quad (1)$$

where $\hat{\mathbf{S}}_i$ is the spin-$\frac{1}{2}$ operator at site i. Here, $J_1, J_2 \leqslant 0$ (ferromagnetic) and $J_d \geqslant 0$ (antiferromagnetic), normalized so that $|J_1| + |J_2| + J_d = 1$. The indices $\langle ij \rangle, \langle\langle ij \rangle\rangle$, and $\langle\langle\langle ij \rangle\rangle\rangle_d$ denote sums over NN and next-NN bonds, and the diagonals of hexagons, respectively (Fig. 1).

In the PF-FRG approach [27–29,40,41], we first rewrite Eq. (1) in terms of pseudofermions as $\hat{\mathbf{S}}_i = \frac{1}{2} \sum_{\alpha\beta} \hat{c}^\dagger_{i,\alpha} \boldsymbol{\sigma}_{\alpha\beta} \hat{c}_{i,\beta}$, $(\alpha, \beta = \uparrow, \downarrow)$, where $\hat{c}_{i,\alpha}$ are the pseudofermion operators, and $\boldsymbol{\sigma}$ are Pauli matrices. This enables us to apply Wick's theorem and develop a diagrammatic technique. To this end, an infrared frequency cutoff Λ is introduced in the fermion propagator. The FRG ansatz (for recent reviews, see, e.g., Refs. [42,43]) then formulates an infinite hierarchy of coupled integrodifferential equations for the evolution of all m-particle vertex functions under the flow of Λ. Within

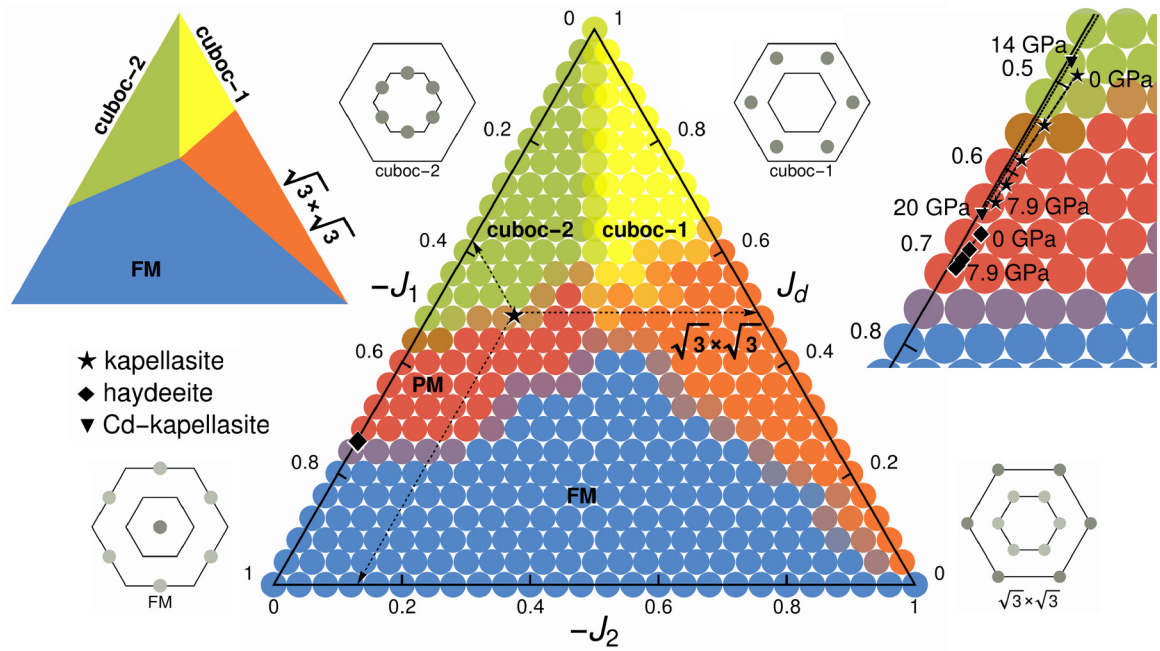

FIG. 2. (Color online) Quantum phase diagram of the J_1-J_2-J_d Heisenberg model as defined in Eq. (1). It features a large paramagnetic (PM) domain for intermediate J_d. The exchange couplings estimated from fitting experimental data for kapellasite and haydeeite are marked [26,38]. The static spin structure factors in the extended Brillouin zone are shown next to each phase. The corresponding classical phase diagram is shown in the upper left. The evolution of the couplings in the different materials under application of pressure, as calculated by *ab initio* methods, is shown in the enlarged region on the right.

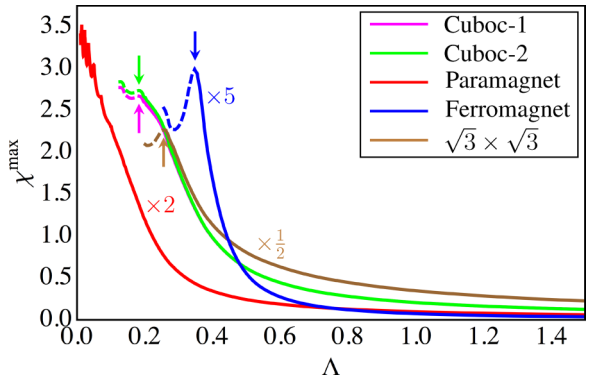

FIG. 3. (Color online) Representative RG flows of the magnetic susceptibilities at the ordering wave vectors of the four ordered regimes of Fig. 2 and the paramagnetic regime. The points at which the solid lines become dashed (marked by arrows) indicate an instability in the flow and express the onset of order. In the smooth flow (red curve) indicating paramagnetism, no such instability is found. The small oscillations below $\Lambda \approx 0.1$ in this flow are due to frequency discretization.

PF-FRG, the truncation of this system of equations to a closed set is accomplished by the inclusion of only two-particle reducible two-loop contributions, which ensures sufficient backfeeding of the self-energy corrections to the two-particle vertex evolution [44]. A crucial advantage of the PF-FRG is that the diagrammatic summation incorporates vertex corrections between all interaction channels, i.e., treats magnetic ordering and disordering tendencies on equal footing. The PF-FRG equations are solved numerically by discretizing the frequency dependencies of the vertex functions and limiting the spatial dependencies to a finite cluster. We used 64 discretized frequencies and a cluster of 432 sites. In the PF-FRG approach, the onset of magnetic long-range order is signaled by a breakdown of the smooth RG flow, whereas a smooth evolution down to $\Lambda \to 0$ (where Λ is the infrared frequency cutoff) indicates PM behavior [27] (Fig. 3). From the effective low-energy two-particle vertex, we obtain the spin-spin correlation function in real space, which we then convert into the momentum-resolved spin susceptibility (see Fig. 4).

Previous applications of the PF-FRG method to frustrated magnets have been extremely successful. In particular, (i) the determined magnetic and nonmagnetic phases of the spin-$\frac{1}{2}$ Heisenberg J_1-J_2 antiferromagnet on the square lattice and the locations of the phase transitions quantitatively agree with DMRG, exact diagonalization, and other methods [27], (ii) the phase diagram of the J_1-J_2-J_3 Heisenberg model on the honeycomb lattice agrees perfectly with exact diagonalization [40,45], (iii) the phase diagram of the Kitaev-Heisenberg model is also correctly determined within the PF-FRG [41,46], in particular, the short range nature of the spin correlations in the Kitaev limit is correctly reproduced, and (iv) the spin structure factor of the NN Heisenberg antiferromagnet on the Kagome lattice in PF-FRG is in very good quantitative agreement with DMRG [9,29], which is of particular relevance to the problem at hand.

For *ab initio* DFT calculations we used the generalized gradient approximation (GGA) functional [47]. Structure optimizations were performed with the projector augmented wave method within the VASP code [48,49], and accurate total energies were calculated using the all-electron FPLO code [50].

Results. The PF-FRG quantum phase diagram of the J_1-J_2-J_d model of Eq. (1) is depicted in Fig. 2. Individual data points are labeled according to which type of phase they belong to in the PF-FRG. For small J_d, FM dominates. For intermediate J_d and large J_2, a $\sqrt{3}\times\sqrt{3}$ order is found which changes into the cuboc-1 order for increasing J_d. The cuboc orders describe 12-sublattice noncoplanar orders in which the spins orient towards the corners of a cuboctahedron [51,52] (that is, along the 12 possible [110] directions). For the domains discussed so far, the quantum phase diagram approximately matches the classical phase diagram of Eq. (1) (Fig. 2). Quantum corrections start to become visible closer to the cuboc-1/cuboc-2 boundary, as J_2 becomes smaller than J_1 (for large J_d). The classical first order transition line between the cuboc-1 and cuboc-2 phases is then replaced by a narrow vertical strip ($J_1 \approx J_2$) in the quantum case, depicted by a merging gradient in Fig. 2, where an effectively $1D$ paramagnetic chain regime is found. As the most important modification to the classical picture, however, an extended PM regime emerges for $J_2/J_1 < 1$ separating the cuboc-2 from the FM domain. Its spin susceptibility profile has a well-defined wave-vector dependence featuring dominant short-distance correlations with soft maxima at cuboc-2 ordering wave vectors and subdominant FM correlations. This type of magnetic fluctuation profile is rather peculiar for a PM phase and fundamentally different from what is found for herbertsmithite [29,30]. As we enter the PM regime from the cuboc-2 phase by lowering J_d, the magnetic correlations change quantitatively but not qualitatively, as is manifest from a comparison of their spin susceptibility profiles in Figs. 4(c)

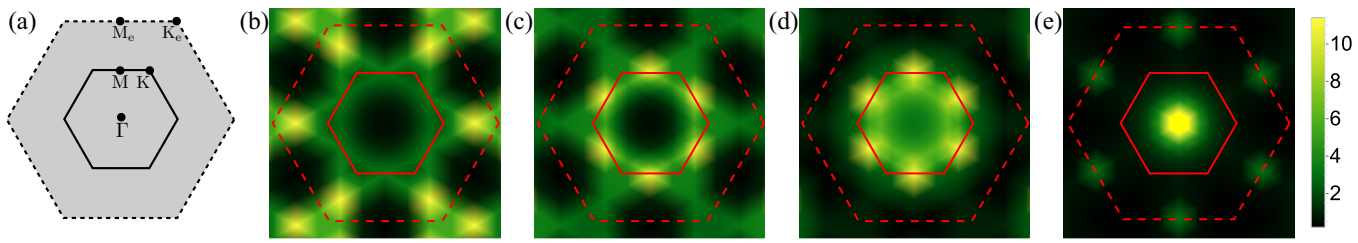

FIG. 4. (Color online) (a) The first (solid line) and extended (dashed line) Brillouin zones of the kagome lattice. (b)–(e) Representative spin susceptibility profiles obtained in PF-FRG for different regimes of the quantum phase diagram in Fig. 2: (b) cuboc-1, (c) cuboc-2, (d) paramagnetic (PM), (e) ferromagnetic (FM).

and Fig. 4(d). The only notable difference is more spectral weight smearing in the PM regime. Within the PM regime, the spin correlations are found to be short-ranged, and calculations of the dimer response function rule out any kind of valence-bond crystal order up to a 36-site cell. Note that the J_1-J_2-J_d model has been recently analyzed by variational Monte Carlo (VMC) [53]. There, in the large J_d regime, noncoplanar cuboc-1 order is absent, and cuboc-2 order is reduced to a small part of the parameter space. Instead, for a significant range of J_d and depending on J_2/J_1, two distinct gapless $U(1)$ chiral spin liquids with a spinon Fermi surface are found over an extended region. As opposed to the PF-FRG, which treats magnetic order and disorder tendencies on the same footing, a certain bias of VMC against cuboc-1 and cuboc-2 orders can be argued for on the basis of the variational wave functions employed. The noncoplanar structure of cuboc-1 and cuboc-2 orders implies that the corresponding chosen Jastrow wave functions are inaccurate as the Jastrow factor does not correctly describe the relevant quantum fluctuations on top of the classical state [53]. On the other hand, PF-FRG does not suffer from this deficiency, and, if anything, may slightly *over*estimate the PM domain.

The location of the high-temperature series expansion estimate of exchange couplings for KL [38] is marked within the center triangle by a star at (0.38,0.13,0.49) in Fig. 2. This is very close to the boundary between the cuboc-2 and the quantum PM phases. Experimentally, KL shows no spin freezing and persistent fluctuations down to 20 mK (by μSR), a diffused continuum of excitations (inelastic neutron scattering), and the divergence of the intrinsic local susceptibility for $T \to 0$ in NMR [54]. The static spin structure factor shows a well-defined wave-vector dependence exhibiting AFM short-range correlations [51,55], consistent with the cuboc-2 pattern. This whole set of experiments has been interpreted in favor of a gapless quantum spin liquid [54] close to the cuboc-2 AFM order. The delicate location of KL might have important experimental implications, in that only moderate modifications in material synthesis or experimental conditions amounting to strain, pressure, defects/impurities, and the imminent presence of different type of anisotropies would lead to significant effects. Slight modifications of the Heisenberg coupling constants could drive kapellasite either into a weak cuboc-2 order or towards a quantum PM phase. As tentatively observed in current experiments, this finding is consistent with the compound exhibiting strong magnetic frustration and significant ordering fluctuation tendencies towards cuboc-2 at the same time. Our PF-FRG calculations show that this kapellasite location yields a critical flow, that is, neither shows a robust and smooth RG flow down to $\Lambda = 0$ that would point at quantum PM nor exhibits a clear signature of an order-induced breakdown.

The location of the linear spin-wave estimate of exchange couplings for haydeeite [26] is marked by the diamond at (0.77,0.0,0.23) in Fig. 2. Remarkably, it is likewise located at the border with the PM regime, but now on the FM side. Experiments [26] suggest a very weak FM order below 4.2 K. From our PF-FRG analysis, ferromagnetic order is weak but unambiguous, and the magnetic fluctuations clearly show FM signatures: a dominant peak at Γ and subdominant peaks at M_e [see Fig. 4(e)].

To summarize, the reported exchange parameters [26,38] place KL and HD on opposite sides of the (arguably most interesting) paramagnetic region. Moreover, it seems like these two compounds, accidentally, are both at or very close to a borderline between two phases. While making them especially intriguing, it also considerably complicates their study. It is therefore highly desirable to be able to modify the same compounds continuously, in order to "traverse" the phase diagram. In principle, there are several ways to do so.

One option is alloying Mg and Zn by creating a mixed compound $Mg_xZn_{1-x}Cu_3(OH)_6Cl_2$ as suggested in Ref. [26]. However, while this proposal creates a system with *average* exchange couplings intermediate between those in KL and HD, in reality it will have random bonds with exchange constants similar to those either in KL or HD and is more likely to freeze into a spin glass state rather than to develop a spin-liquid phase. Besides, chemical substitution of Zn by Mg naturally affects J_d, but the effect on J_1 is harder to predict.

These considerations lead us to propose alternative options without introducing additional disorder. For that, we need first to exercise some caution when using the experimental numbers. Indeed, Refs. [26,38] are complementary in terms of methodology used to extract the exchange coupling constants; Ref. [38] relies on magnetometry/calorimetry while Ref. [26] does a spin-wave analysis. In both cases, and especially in HD, actual samples have considerable excess of Zn or Mg, substituting for Cu. Each missing Cu creates four incompletely frustrated spins, which may alter the results compared to the stoichiometric compound. While the reported parameters for HD are consistent with a FM ground state, the experimental data [26] looks more complicated than that. Indeed, the ordered moment from neutron scattering was estimated to be $\lesssim$0.2 μ_B [26], while the saturation moment from magnetization was 0.83 [26] or 1.0 μ_B [25], and the spontaneous ordered moment is 0.02 μ_B [24] or less [25]. The Curie-Weiss effective moment is 1.83 μ_B [24], consistent with an ordered moment greater than 1 μ_B. A 40 times difference between the saturation and spontaneous magnetization is highly unusual, and so is the discrepancy between spontaneous and neutron-measured moments. While this has been vaguely ascribed to frustration [26], the "frustration parameter," usually defined as the ratio of the mean field T_{CW} and frustration-suppressed T_N, is in fact less than one here. The magnetic susceptibility starts growing with cooling below 5 K but does not diverge at the putative $T_C = 4.2$ K and instead starts flattening out below 4 K. Overall, the magnetic behavior described in Ref. [26] is more typical for canted antiferromagnets than for ferromagnets. On the other hand, an independent study [25] found much larger magnetic moment and stronger ferromagnetic behavior.

Given the experimental situation, we decided to address the question theoretically by performing DFT+U calculations (see Supplemental Material). We used the FPLO program with $U = 6$–8 eV, using the fully-localized double counting scheme, orthogonal projection of $3d$ density, and gradient corrections in the DFT functional, and we found that, in agreement with previous observations [32], this setup gives the closest agreement with the experiment for KL. As discussed in detail in the Supplemental Material, the exchange coupling constants in these materials are not only small, but they also

depend on the technical details of the setup (we remind the reader that while DFT is a first principles method, DFT+U is not), which accounts, for instance, for the difference between Refs. [32] and [55]. On the other hand, the trends in the dependence of the exchange parameters on the geometry and chemistry in these compounds are quite robust, and therefore such calculations can be used as a guidance for modifying existing materials in order to steer them toward one or another magnetic phase.

With this setup, using reported crystal structures (and optimized positions of hydrogen, since these are not known experimentally) we obtained for KL $(J_1, J_2, J_d) = (-12.5, -0.55, 16.1)$ K, corresponding to (0.43,0.02,0.55). This is rather close to $(-12, -4, 15.6)$ K [38], albeit a bit deeper in the cuboc-2 phase. For HD we find $(-21.2, 0.57, 12.8)$ K, or (0.61,0.02,0.37), placing it in the PM regime (see inset in Fig. 2). By comparing calculations for the same structure, but substituting Zn for Mg, or for the same composition but different structure, we found, not surprisingly, that J_1 is predominantly (80–90%) controlled by the structure and J_d by the bridging element. The smaller Cu-O-Cu angle in HD of 104.98° vs 105.84° in KL results in a larger value for J_1, while the additional hopping path *via* semicore Zn 3*d* states provides a larger J_d. The principal discrepancy with the experimental values appears to be the overestimation of J_d in HD. Regardless of whether this is an experimental problem (e.g., imperfect samples) or theoretical (e.g., overestimation of Mg-O $sp\sigma$ hopping), the trends in the dependence of the exchange parameters with respect to both structural and chemical changes are well reproduced. Having identified the origin of the behavior of J_1 and J_d, we propose two recipes for sampling the phase diagram.

The first option is to apply pressure, keeping the chemical compositions. To investigate this avenue, we have calculated the structures of KL and HD at experimental volumes and at compressions up to 12% (Fig. 5). These compressions correspond to pressures of ≈7.9 GPa for both KL and HD, which is experimentally accessible. In both cases, the Cu-O-Cu angle decreases systematically, and J_1 increases by up to 140% (KL) and 80% (HD), as shown in Fig. 5. Thus, by applying pressure we should be able to drive KL into the PM regime, and even approach the boundary with the FM phase, while applying pressure to HD will drive it deeper into the FM regime.

The second option combines both structural and chemical changes. One can preserve homogeneity by substituting Zn in KL with Cd. Due to the larger ionic radius, this substitution may be difficult to realize and might require high-pressure synthesis. Indeed, our calculations show that while such a compound would be locally stable, the Cu-Cd plane would be considerably expanded and the Cu-OH-Cu angle would flatten to 112°–113°, which renders J_1 antiferromagnetic [37]. This compound, however, would also be highly compressible and would return to a structure similar to KL at a pressure of about 20 GPa. One expects that J_1 should already be ferromagnetic

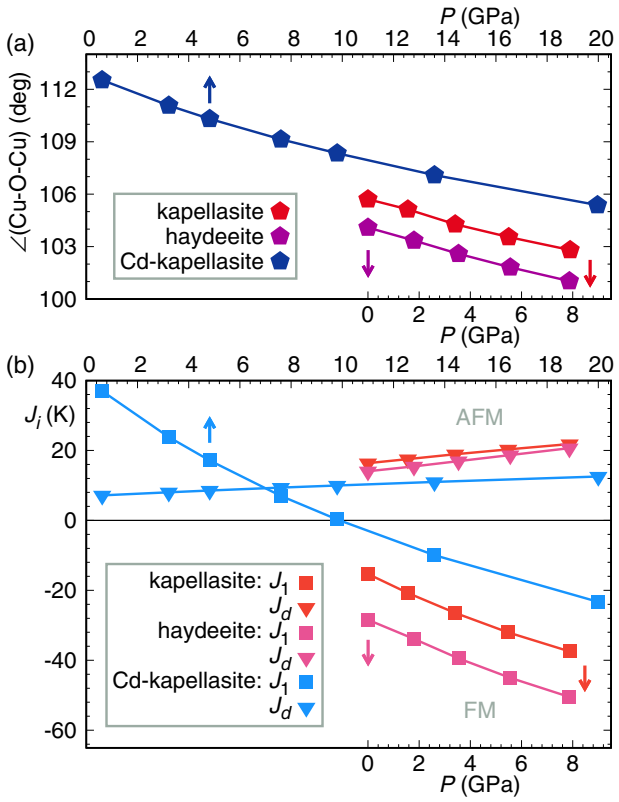

FIG. 5. (Color online) (a) Predicted evolution of Cu-O-Cu angles as a function of pressure for kapellasite, haydeeite, and the hypothetical Cd-kapellasite. (b) Pressure induced changes in the two dominant exchange coupling parameters J_1 and J_d for the three compounds.

at this pressure, while at the same time, we note that since the 5*d* level in Cd lies considerably lower compared to the 4*d* level in Zn, the J_d is expected to reduce. Both conjectures are confirmed by our calculations. Indeed, at $P = 20$ GPa the representative point in the phase diagram appears close to HD at $P = 0$, while at $P = 13.6$ GPa it is close to KL at $P = 0$ (Fig. 2). Thus, synthesizing $CdCu_3(OH)_6Cl_2$ and applying external pressure provides us a vehicle to traverse a vast extent of the phase diagram encompassing a large range of J_d, especially deep into the paramagnetic phase.

Acknowledgments. We thank F. Becca, S. Bieri, V. Khanna, C. Lhuillier, T. Neupert, D. Poilblanc, H. Rosner, and R. Suttner for useful discussions. The work was supported by the European Research Council through ERC-StG-TOPOLECTRICS-Thomale-336012. I.I.M. was also supported by the Office of Naval Research through the Naval Research Laboratory's Basic Research Program. H.O.J. and R.V. thank the DFG (Deutsche Forschungsgemeinschaft) for financial support through SFB/TRR 49 and FOR 1346, and Y.I., M.G., and R.T. received financial support through SFB 1170. J.R. is supported by the Freie Universität Berlin within the Excellence Initiative of the German Research Foundation.

[1] I. Pomeranchuk, Zh. Eksp. Teor. Fiz. **11**, 226 (1941).
[2] L. Balents, Nature (London) **464**, 199 (2010).
[3] R. R. P. Singh and D. A. Huse, Phys. Rev. B **76**, 180407 (2007).
[4] Y. Ran, M. Hermele, P. A. Lee, and X.-G. Wen, Phys. Rev. Lett. **98**, 117205 (2007).
[5] H. Nakano and T. Sakai, J. Phys. Soc. Jpn. **80**, 053704 (2011).

[6] A. M. Läuchli, J. Sudan, and E. S. Sørensen, Phys. Rev. B **83**, 212401 (2011).
[7] Y. Iqbal, F. Becca, and D. Poilblanc, Phys. Rev. B **83**, 100404 (2011); **84**, 020407 (2011).
[8] S. Yan, D. A. Huse, and S. R. White, Science **332**, 1173 (2011).
[9] S. Depenbrock, I. P. McCulloch, and U. Schollwöck, Phys. Rev. Lett. **109**, 067201 (2012).
[10] H.-C. Jiang, Z. Wang, and L. Balents, Nat. Phys. **8**, 902 (2012).
[11] S. Capponi, V. R. Chandra, A. Auerbach, and M. Weinstein, Phys. Rev. B **87**, 161118 (2013).
[12] Y. Iqbal, F. Becca, S. Sorella, and D. Poilblanc, Phys. Rev. B **87**, 060405 (2013).
[13] Z. Y. Xie, J. Chen, J. F. Yu, X. Kong, B. Normand, and T. Xiang, Phys. Rev. X **4**, 011025 (2014).
[14] M. Punk, D. Chowdhury, and S. Sachdev, Nat. Phys. **10**, 289 (2014).
[15] Y. Iqbal, D. Poilblanc, and F. Becca, Phys. Rev. B **89**, 020407 (2014).
[16] R. Nandkishore, J. Maciejko, D. A. Huse, and S. L. Sondhi, Phys. Rev. B **87**, 174511 (2013).
[17] I. I. Mazin, H. O. Jeschke, F. Lechermann, H. Lee, M. Fink, R. Thomale, and R. Valentí, Nat. Commun. **5**, 4261 (2014).
[18] M. P. Shores, E. A. Nytko, B. M. Bartlett, and D. G. Nocera, J. Am. Chem. Soc. **127**, 13462 (2005).
[19] T.-H. Han, J. S. Helton, S. Chu, D. G. Nocera, J. A. Rodriguez-Rivera, C. Broholm, and Y. S. Lee, Nature (London) **492**, 406 (2012).
[20] W. Krause, H.-J. Bernhardt, R. S. W. Braithwaite, U. Kolitsch, and R. Pritchard, Mineral. Mag. **70**, 329 (2006).
[21] R. H. Colman, C. Ritter, and A. S. Wills, Chem. Mater. **20**, 6897 (2008).
[22] T. Malcherek and J. Schlüter, Acta Crystallogr., Sect. B: Struct. Sci. **63**, 157 (2007).
[23] J. Schlüter and T. Malcherek, Neues Jahrbuch für Mineralogie - Abhandlungen **184**, 39 (2007).
[24] R. Colman, A. Sinclair, and A. Wills, Chem. Mater. **22**, 5774 (2010).
[25] S. Chu, J. Phys.: Conf. Ser. **273**, 012123 (2011).
[26] D. Boldrin, B. Fåk, M. Enderle, S. Bieri, J. Ollivier, S. Rols, P. Manuel, and A. S. Wills, Phys. Rev. B **91**, 220408 (2015).
[27] J. Reuther and P. Wölfle, Phys. Rev. B **81**, 144410 (2010).
[28] J. Reuther and R. Thomale, Phys. Rev. B **83**, 024402 (2011).
[29] R. Suttner, C. Platt, J. Reuther, and R. Thomale, Phys. Rev. B **89**, 020408 (2014).
[30] T. Han, S. Chu, and Y. S. Lee, Phys. Rev. Lett. **108**, 157202 (2012).
[31] G. Misguich and P. Sindzingre, Eur. Phys. J. B **59**, 305 (2007).
[32] H. O. Jeschke, F. Salvat-Pujol, and R. Valentí, Phys. Rev. B **88**, 075106 (2013).
[33] Y. Iqbal, D. Poilblanc, and F. Becca, Phys. Rev. B **91**, 020402 (2015).
[34] Y. Iqbal, F. Becca, and D. Poilblanc, New J. Phys. **14**, 115031 (2012); F. Becca, W.-J. Hu, Y. Iqbal, A. Parola, D. Poilblanc, and S. Sorella, J. Phys.: Conf. Ser. **640**, 012039 (2015).
[35] P. Mendels, F. Bert, M. A. de Vries, A. Olariu, A. Harrison, F. Duc, J. C. Trombe, J. S. Lord, A. Amato, and C. Baines, Phys. Rev. Lett. **98**, 077204 (2007).
[36] M. Fu, T. Imai, T.-H. Han, and Y. S. Lee, Science **350**, 655 (2015).
[37] See Supplemental Material at http://link.aps.org/supplemental/10.1103/PhysRevB.92.220404 for a discussion on the origin of exchange parameters, and details of *ab initio* calculations.
[38] B. Bernu, C. Lhuillier, E. Kermarrec, F. Bert, P. Mendels, R. H. Colman, and A. S. Wills, Phys. Rev. B **87**, 155107 (2013).
[39] E. Kermarrec, A. Zorko, F. Bert, R. H. Colman, B. Koteswararao, F. Bouquet, P. Bonville, A. Hillier, A. Amato, J. van Tol, A. Ozarowski, A. S. Wills, and P. Mendels, Phys. Rev. B **90**, 205103 (2014).
[40] J. Reuther, D. A. Abanin, and R. Thomale, Phys. Rev. B **84**, 014417 (2011).
[41] J. Reuther, R. Thomale, and S. Trebst, Phys. Rev. B **84**, 100406 (2011).
[42] W. Metzner, M. Salmhofer, C. Honerkamp, V. Meden, and K. Schönhammer, Rev. Mod. Phys. **84**, 299 (2012).
[43] C. Platt, W. Hanke, and R. Thomale, Adv. Phys. **62**, 453 (2013).
[44] A. A. Katanin, Phys. Rev. B **70**, 115109 (2004).
[45] A. F. Albuquerque, D. Schwandt, B. Hetényi, S. Capponi, M. Mambrini, and A. M. Läuchli, Phys. Rev. B **84**, 024406 (2011).
[46] J. Chaloupka, G. Jackeli, and G. Khaliullin, Phys. Rev. Lett. **105**, 027204 (2010).
[47] J. P. Perdew, K. Burke, and M. Ernzerhof, Phys. Rev. Lett. **77**, 3865 (1996).
[48] G. Kresse and J. Hafner, Phys. Rev. B **47**, 558(R) (1993).
[49] G. Kresse and J. Furthmüller, Phys. Rev. B **54**, 11169 (1996).
[50] K. Koepernik and H. Eschrig, Phys. Rev. B **59**, 1743 (1999); http://www.FPLO.de.
[51] L. Messio, C. Lhuillier, and G. Misguich, Phys. Rev. B **83**, 184401 (2011).
[52] S.-S. Gong, W. Zhu, L. Balents, and D. N. Sheng, Phys. Rev. B **91**, 075112 (2015).
[53] S. Bieri, L. Messio, B. Bernu, and C. Lhuillier, Phys. Rev. B **92**, 060407 (2015).
[54] B. Fåk, E. Kermarrec, L. Messio, B. Bernu, C. Lhuillier, F. Bert, P. Mendels, B. Koteswararao, F. Bouquet, J. Ollivier, A. D. Hillier, A. Amato, R. H. Colman, and A. S. Wills, Phys. Rev. Lett. **109**, 037208 (2012).
[55] O. Janson, J. Richter, and H. Rosner, Phys. Rev. Lett. **101**, 106403 (2008).